Nepomuceno, E.; Sena-Cruz, J.; Correia, L.; D'Antino, T. (2021) "Review on the bond behavior and durability of FRP bars to concrete." Construction and Building Materials, 287: 123042, 14 pp. DOI: 10.1016/j.conbuildmat.2021.123042

REVIEW ON THE BOND BEHAVIOR AND DURABILITY OF FRP BARS TO CONCRETE

Eduarda Nepomuceno[1], José Sena-Cruz[1]*, Luís Correia[1], Tommaso D'Antino[2]

[1]ISISE / IB-S, University of Minho, Department of Civil Engineering, Campus de Azurém, 4810-058 Guimarães, Portugal

[2]Politecnico di Milano, Department of Architecture, Built Environment, and Construction Engineering, Via Ponzio 31, 20133 Milan, Italy

* E-mail: jsena@civil.uminho.pt; *Corresponding author*

Abstract: In the past two decades, the use of Fiber Reinforced Polymer (FRP) bars in reinforced concrete structures has been increasing, replacing conventional steel reinforcement, especially in areas with adverse environmental conditions. This paper presents a literature review on the bond behavior of FRP bars to concrete, which includes studies on their (i) instantaneous and (ii) long-term (durability) properties. This work also included a database created from the collection of experimental data in the existing literature, with results from a total of 1002 pullout tests, intended to clarify the most relevant parameters that influence the bond of FRP bar to concrete. The analysis conducted on the database yielded the conclusion that FRP bar exhibits a good performance as reinforcement in concrete structures. Moreover, the collected data allowed the development of FRP bar to concrete bond (durability) long-term predictions considering the type of exposure environment.

Keywords: Concrete; Fiber reinforced polymer; FRP bar; Bond strength; Durability; Long-term prediction; Environment effect.

Nepomuceno, E.; Sena-Cruz, J.; Correia, L.; D'Antino, T. (2021) "Review on the bond behavior and durability of FRP bars to concrete." Construction and Building Materials, 287: 123042, 14 pp. DOI: 10.1016/j.conbuildmat.2021.123042

1. INTRODUCTION

Reinforced concrete structures with steel bars are widely used in engineering applications since late XIX century. Despite that, exposing these structures to aggressive environments, such as de-icing salts or seawater, can result in severe degradation of the structure due to corrosion of the steel reinforcement. More recently, the use of Fiber Reinforced Polymer (FRP) bars as internal reinforcement in concrete structures appeared as a promising alternative to steel bars. Among the main advantages of FRP bars with respect to steel bars, the following stand out: (i) high corrosion resistance, (ii) high longitudinal tensile strength, (iii) lightweight, (iv) low thermal conductivity, and (v) good fatigue behavior (depending on the type of fiber) [1 – 3]. For this reason, researchers have turned their efforts to study the use of FRP bars as reinforcement in concrete and, thus, increase the utilization of this promising material. Because of these efforts, e.g., the American Concrete Institute (ACI), the Canadian Standards Association (CSA) and the National Research Center of Italy (CNR) published the guidelines ACI 440.1R-15 [4], CSA S806-12 [5] and CNR-DT 203-06 [6], respectively.

The success of this material as reinforcement in concrete structures depends on the understanding of the bond between FRP bars and concrete, including short and long-term behavior (durability aspects). Figure 1 presents a representative scheme of a typical test setup for the study of bond behavior. The specimen is normally composed of a concrete block where, prior the casting phase, the FRP bar is installed. The pull-push configuration is usually adopted, where the bar is pulled while the concrete block is restrained. Typically, the FRP bar is bonded to concrete only for a certain length. The instrumentation includes the measurement of the applied pullout force (F) and the relative displacement between the concrete block and the loaded (s_l) and free end (s_f) sections (slips). Three LVDTs spaced at 120° should be used to measure the axial displacement of the FRP bar. Given the configuration of the bond specimen, the elastic deformation of the FRP bar between the loaded end section and the point where the s_l is registered should be accounted for. Finally, in order to guarantee the test stability, displacement control should be adopted, by using the LVDTs at the loaded end.

Since many parameters can influence the bond behavior, several issues remain unanswered for a complete comprehension of the bond between FRP bars and concrete. Among these issues, the bond strength can be mentioned. In the context of this work, the bond strength (or maximum average bond stress) is defined as the ratio between the maximum pullout force (F) and the contact area between the FRP bar and concrete, assuming that the

shear stresses developed along the embedded length are constant, as per e.g. ASTM D7913/D7913M-14 [7] or ACI 440.3R-04 [8]. The bond strength is commonly determined throughout pullout tests and beam tests. This paper uses data from pullout tests. The specimens of pullout tests (bond specimens) are comprised by FRP bars embedded in concrete. From the collated database, specimens cast individually [9 – 31] or grouped [32, 33] were identified. Embedded lengths in different positions were also identified, on the edge [10, 12, 17, 19 – 31] or in the middle [9, 11, 13 – 16, 18, 32, 33] of the specimens.

Studies were carried out to deepen the knowledge regarding the composite action between FRP bars and concrete. Most of these studies are focused on the short-term investigation of bond behavior, including the FRP bar to concrete bond strength. These works identified several parameters that influence the bond behavior, namely:

i. Type of fiber: can affect the stiffness, changing the ascending branch of the bond stress-slip curve, e.g. [9, 10];

ii. Embedded length: studies carried out, e.g. [11 – 13], indicate that when the embedded length increases, the bond strength decreases due to the non-linear evolution of the bond stresses along the bond length;

iii. Bar diameter: investigations on the diameter change indicate that when increases, the bond strength decreases, e.g. [10 – 13];

iv. Type of surface: the external surface of the FRP bar plays a critical role in the shear stress transfer and resisting mechanisms of the FRP bar to concrete, as referred by [11, 14 – 16];

v. Concrete compressive strength: several studies, e.g. [10, 11, 17, 32], reported changes in the slip, failure mode, and bond strength when concretes with different compressive strengths are used.

The studies on the short-term bond behavior also tried to identify the different failure modes that may occur between FRP bars and concrete, namely: (i) pullout, (ii) concrete splitting, and (iii) peeling. Among these, the first two are the most commonly observed, and also occur in pullout tests with steel bars. Further analyzes of the failure mode were performed by [10, 11, 17, 18]. The authors identified the differences between the failure mode with steel bars and FRP bars through visual examinations. For deformed steel bars, the failure occurs on the surface between the steel bar and the concrete. Then, cracks in the concrete are developed around the steel bar; with increased stress, the concrete crushes against the bar ribs, causing the failure. In this way, the bond failure is related to concrete failure, and the bond strength appears to be governed by the concrete mechanical properties. On the

other hand, FRP bars failure can occur on the surface between the FRP bar matrix and the concrete, or the surface between the FRP bar matrix and the FRP bar fiber due to the peeling of the bar surface layer (sleeve). For the second case (matrix-fiber interface), the shear stresses between the bar fibers and the bar matrix seem to control the bond strength, indicating that the bond strength depends more on the FRP bar characteristics than on the compressive strength of the concrete, particularly for concretes medium/high compressive strength values.

In order to broaden the understanding of the bond behavior between FRP bars and concrete, an empirical model was presented by Okelo and Yuan [34] to predict the bond strength. In this model, the bond strength is considered to increase proportionally to the 0.5 power of concrete compressive strength and decreases as the reinforcing bar diameter increases. On the other hand, Lee et al. [17] proposed that the bond strength between GFRP bars and concrete increases proportionally to the 0.3 power of concrete compressive strength. Despite the significant advances in understanding the bond behavior of FRP bar to concrete, critical aspects still deserve attention. Analytical models for accurately predicting the bond strength are still scarce, and more studies should be conducted.

Some other studies were devoted to the durability of the bond between FRP bar and concrete. Different methods were used in these investigations to accelerate the aging of bond specimens through exposure to different environmental conditions, considered aggressive for reinforced concrete structures. Accelerated aging is meant to reproduce, in relatively short periods, the aging caused by real environment actions, which would take years to complete. Saline, alkaline, acid, and thermal environmental conditions are commonly employed. From the search carried out, 13 studies were found in the literature concerning this topic [14, 19 – 30]. Although studies on the bond between FRP bars and concrete are increasing, only a few addressed the bond strength long-term prediction (i.e., the bond strength durability), which appears as a significant gap in the existing literature.

This paper aims to give new insights on the durability of the bond of FRP bars to concrete, based on the existing produced data. For this purpose, a database of 1002 bond specimens has been built from the literature collection of experimental data. It includes 438 pullout test results of specimens exposed to the most severe environmental conditions, namely: (i) acid solution, (ii) alkaline solution, (iii) saline solution, (iv) immersion in water, (v) elevated temperature in a dry environment, (vi) elevated temperature in a dry environment followed by immersion

in water, (vii) elevated temperature in a dry environment followed by immersion in saline solution and (viii) thermal cycles.

The paper is divided into four main parts. Section 2 presents the main significant published works on the durability aspects of FRP bars to concrete. Then, in Section 3, the database created from the data collated is introduced. In Section 4, an analysis of the abovementioned database and a proper discussion is carried out. Finally, long-term predictions for adverse environments are proposed in Section 5.

2. REVIEW ON DURABILITY ASPECTS OF FRP BARS TO CONCRETE

The durability of concrete structures reinforced with FRP bars depends on (i) the durability of the constituent materials (concrete and FRP bars) and on (ii) the durability of bond between concrete and FRP bars. In the context of civil engineering applications, the principal environmental degradation factors are moisture, thermal effects, UV radiation, and chemicals. The durability of concrete is well established, e.g. [35], while for FRP bars the alkaline environment, moisture, and thermal effects are identified as critical factors [36]. Even though alkali-resistant (AR) glass fibers have shown good durability to alkaline environment (such as concrete), their use in GFRP bars is still limited due to the elevated cost - E-Glass fiber reinforcement is the most used one. Moisture, through a diffusion process at the molecular level, mainly affects the matrix causing plasticization, strength decrease, and reduction of the value of the glass transition temperature. The modulus of elasticity and strength of FRP bars decrease with increasing temperature. This behavior is mainly caused by the significant changes of the mechanical properties of the matrix when temperature reaches values close or above the glass transition temperature of the matrix, while the fibers do not significantly change their properties [36]. Typical values of fiber content in FRP bars vary between 60 and 80%.

Studies available in the literature that investigated the FRP bars to concrete bond behavior usually simulated long-term conditions by exposing the specimens to harsh environments. Zhou et al. [26, 27] evaluated the durability of the bond between glass fiber reinforced polymer (GFRP) bars and concrete. In this investigation, bond specimens were subjected to several environmental conditions (accelerated aging tests), namely immersion in tap water, acid solution (pH = 2, pH = 3, and pH = 4), alkaline solution (pH = 13.5), and saline solution (NaCl, 7%), with exposure times up to 90 days at room temperature. At the end of the exposure time, the authors identified that the most significant reduction in bond strength between GFRP bars and concrete occurred in specimens conditioned into

the acid environment (pH = 2) for 75 days, with a bond strength reduction of 22%. Based on the results experimentally obtained, the authors proposed a service life prediction of the bond strength using a modified Arrhenius equation and a modified time shift factor (TSF) method, considering the pH differences. Retention of 84% of bond strength of a reinforced concrete structure with GFRP bars exposed to an external environment with acid rain (pH = 5.6) for 34 years of service life was obtained.

Dong et al. [28] conducted a study with more than 100 pullout tests of specimens subjected to immersion in seawater, with exposure periods up to 2 months and temperatures ranging from 25 °C to 55 °C (temperatures below the FRP glass transition temperature, which usually ranges between 93 °C and 120 °C [4]). The authors also evaluated the influence of the type of resin used in the FRP bar. Immersion in seawater caused a maximum bond strength reduction of approximately 13% for FRP bars with vinyl ester resin. In contrast, for FRP bars with epoxy resin, no relevant changes in bond strength were observed. The Arrhenius equation and the TSF method were used to develop long-term predictions of the bond strength. Bond strength retentions above 93%, 78%, and 47% were found for dry, moist (concrete not constantly in contact with seawater), and saturated (concrete constantly in contact with seawater) conditions, respectively, after 50 years of service life.

Likewise, Yan and Lin [29] analyzed the long-term bond durability between GFRP bars and concrete conditioned into seawater at 50 °C and 70 °C. Using the time shift factor method, for 75 years of service life, bond strength retentions of 95%, 90%, and 67% for dry, moist, and saturated conditions, considering warm regions under 40 °C were predicted.

More recently, Hassan et al. [30] developed studies on the durability of basalt FRP bars (BFRP) to concrete bond. In this study, the authors exposed the bond specimens to an alkaline solution for periods up to 6 months and temperatures ranging from 40 °C to 60 °C. After six months of immersion in alkaline solution, the authors observed a maximum loss in the bond strength of 16% at a temperature of 40 °C. The authors used the *fib* Bulletin 40 [1] method to predict long-term bond retention. For dry, moist, and saturated conditions, the predicted bond strength retentions were 82%, 76%, and 71%, respectively, over 50 years of service.

3. DATABASE

A database containing 1002 pullout test results was created gathering information from the existing literature [9 – 33]. Table 1 includes some information about the parameters analyzed, namely (i) fiber type, (ii) embedded length, (iii) diameter, (iv) surface treatment, (v) type of environmental condition exposure, (vi) compressive strength of concrete, and (vii) bond strength.

The collected pullout test results included different types of fiber composing the FRP bar, namely basalt (BFRP), carbon (CFRP), and glass (GFRP). The diameter (Ø) of the FRP bars ranged from 7 mm to 29 mm, while the embedded length varied between 2Ø to 20Ø. The different surface treatments of FRP bars were grouped as sand-coated with a deformed surface (SC + DS), deformed surface (DS), sand-coated (SC), and smooth (SM). Bond durability of FRP bars to concrete was analyzed through bond specimens that were exposed to specific environmental conditions, namely: immersion in acid solution (AC), alkaline solution (AK), saline solution (SA), water (WA), exposure to elevated temperature in a dry environment (HT), elevated temperature in a dry environment followed by immersion in water (HWA) or in saline solution (HSA), and thermal cycles (TC). In the case of TC, the temperatures varied between −20 °C and 60 °C, in periods ranging from 7 to 107 days of exposure, while the other conditions were tested at temperatures from 20 °C to 80 °C, with exposure of 15 to 240 days (5760 hours of exposure).

Considering the large number of data collected and the different sources where the data came from, a significant variation in the used materials was observed. Thus, for the data collected, a wide variation was observed in the following parameters: Young's modulus of FRP bars varied between 31 GPa and 170 GPa, the bond strength between 0.1 MPa and 67.8 MPa, and the compressive strength of concrete between 12 MPa and 170 MPa. As referred before, concrete strength plays an important role in the bond between FRP bar and concrete. Given the considerable variation of the concrete classes used in the data collected, in the scope of the present work and for specific analyses, the bond strength values were normalized respect to the concrete compressive strength, according to Eq. (1). It should be highlighted that although the use of Eq. (1) may be arguable, especially when different failure modes are obtained, a similar methodology has been previously used in the literature, e.g. [10, 15, 19, 20, 25, 29]:

$$\tau_{\mathrm{n}} = \frac{\tau_{\max}}{\sqrt{\frac{f_{\mathrm{cm}}}{1\ \mathrm{MPa}}}} \tag{1}$$

In Eq. (1), τ_n is the normalized bond strength in [MPa], τ_{max} is the bond strength in [MPa], and f_{cm} is the compressive strength of concrete in standard cylinders (150/300 mm) in [MPa].

4. DATA ANALYSIS AND DISCUSSION

The collected data analysis was divided into two parts: (i) unconditioned bond specimens to assess the short-term (instantaneous) bond behavior and, (ii) conditioned specimens to determine the long-term bond durability.

4.1 Unconditioned specimens

In the first phase, parameters that influence the short-term bond behavior were evaluated. Thus, the unconditioned bond specimens were used to analyze the influence of several parameters on the bond strength, namely: (i) the type of fiber, (ii) the embedded length, (iii) the diameter of the bar, and (iv) the type of surface. A study of the failure modes between the FRP bar and concrete was also carried out. Finally, the bond strength was assessed analytically.

4.1.1 Influence of the fiber type

Among the three types of FRP bars, basalt (BFRP), carbon (CFRP), and glass (GFRP), the latter is the most widely used due to its cost-effectiveness when compared to BFRP and CFRP. For unconditioned bond specimens, 354, 97, and 113 used GFRP, BFRP, and CFRP bars, respectively.

Figure 2 shows the influence of the fiber type on the normalized bond strength. Since the bar stiffness also influences the bond strength, as reported by, e.g. [9, 10], Figure 3 includes the bar stiffness influence on FRP fiber type analysis. High values of coefficients of variation (CoV) can be observed both in Figure 2 and Figure 3, reaching a maximum of 73%. Regardless of the type of analysis, BFRP bars yield to higher values of bond strength than GFRP and CFRP bars. When the bar stiffness is considered in the analysis, CFRP bars present the lowest performance, being 51% and 65% inferior to their counterparts, GFRP and BFRP, respectively. This observation can be explained by the much higher Young's modulus of CFRP and the absence of FRP bar rupture in the pullout tests.

4.1.2 Influence of the embedded length

From the several studies collected, 15 different embedded lengths were found, ranging from 2Ø to 20Ø. The most common embedded length is 5Ø, representing 48% of the validated results among unconditioned bond specimens. The reason for the use of 5Ø can be found in the suggested value by guidelines for bond characterization of FRP bars to concrete, e.g., CSA S806-12 [5], ACI 440.3R-04 [8], and ASTM D7913/D7913M-14 [7].

Figure 4 shows the influence of the embedded length on the normalized bond strength for different embedded lengths. In this chart, the embedded lengths were organized in 8 intervals. Despite the high magnitude of coefficients of variation observed, they are much lower than those in the previous analysis. From this figure, it is clear that the normalized bond strength presents a tendency to decrease with the embedded length. The present observation was also reported by [11 – 13]. Two phenomena are associated with this behavior: (i) the nonlinear distribution of bond stresses along the embedded length, since the local bond-slip law is usually composed of an ascending branch up to the peak, followed by a descending branch; and (ii) the Poisson's ratio effect, which due to the elongation of the bar in the longitudinal direction, causes a reduction in its diameter (radial direction). As a result, there is a decrease of friction effects along the length, which is not constant.

Figure 5 presents an exponential fit of the relationship between the normalized bond strength and the embedded length, according to Eq. (2). The values of a and b were determined using a non-linear regression analysis, which provided $a = 3.621$ and $b = -0.08173$. From this fitting, a coefficient of determination (R^2) of 0.2856 was obtained. The low value of R^2 is due to the large dispersion of data, also generating a high value of root mean square error (RMSE), equal to 0.889. Despite that, from these results, it seems that the bond strength is inversely proportional to the embedded length.

$$\tau_{\mathrm{n}} = a \times exp^{b \times Lb} \tag{2}$$

From these results, it became clear that the embedded length significantly influences the bond strength. For this reason, in the subsequent analyzes, only results with an embedded length (Lb) of 5Ø were considered. As mentioned earlier, the embedded length of 5Ø is suggested by the guidelines CSA S806-12 [5], ACI 440.3R-04 [8], and ASTM D7913/D7913M-14 [7] for bond characterization of FRP bars to concrete. Moreover, given the reduced value of the Lb, the bond strength calculated as the mean value of the shear stresses developed along the embedded length can be considered an acceptable estimation.

4.1.3 Influence of the FRP bar diameter

From the collected data, FRP bar diameters range between 7 mm and 29 mm. Some authors [10 – 13] refer that the increase in the bar diameter leads to a reduction in the bond strength. Assessments of bond stress-slip relationships indicate that the pre-peak curve shows higher stiffness when smaller diameters are considered. It is also suggested that, during the concrete curing process, bars with large diameters accumulate more air pores around them than bar with small diameter, reducing the contact surface between the concrete and the bar.

Figure 6a and b show the relationship between the FRP bar diameter and the normalized bond strength and between the FRP bar diameter and the bond strength, respectively. Results show no clear trend of the FRP bar diameter influence on the bond strength.

4.1.4 Influence of the FRP bar surface treatment

Three main mechanisms are responsible for stress transfer between the bar and concrete. The first is the chemical adhesion, characterized by a resistance that opposes to the separation between materials. The second is the mechanical interlocking related to the bar surface deformations that mobilize localized forces caused by relative displacements. Finally, there is the frictional bond caused by shear stresses that arise from the contact between the concrete and the bar. In this sense, the configuration of the bar surface is of great importance for a good bond performance. For this reason, to enhance the bond performance, several techniques can be used, including surface deformations or sand coating, or a combination of both techniques [1, 37].

FRP bars are manufactured with different surface configurations. In this analysis, the surfaces were organized into four main groups, namely: (i) sand-coated with a deformed surface (SC + DS), (ii) deformed surface (DS), (iii) sand-coated (SC), and (iv) smooth (SM). For the group of unconditioned specimens, with an embedded length of 5Ø, 91 SC + DS, 101 DS, 62 SC, and 18 SM are available for analysis. Figure 7 presents the averages of the normalized bond strength obtained per type of surface. From this figure it becomes clear that the surface configuration plays a crucial role in the bond strength. On average, FRP bars with surface treatment presents a normalized bond strength approximately 140% higher than that of smooth bars.

4.1.5 Failure modes

Figure 8 shows the failure modes observed for unconditioned specimens. From the collected database, 4 failure modes were observed, namely: (i) pullout, (ii) concrete splitting, (iii) peeling off, and (iv) bar rupture, among which the pullout failure represents 71% of the obtained results. The bar rupture was observed in only two works [13, 32], and the failures were attributed to either long embedded lengths (> 15Ø) or misalignment of the bar during the test. In this situation, the tensile strength of the bar was achieved before the bond strength being mobilized.

The interface where failure occurs depends on the stresses developed in the specimen. According to Lee et al. [17], when the shear strength between concrete and FRP matrix (typically the external face of FRP bars is rich in resin) is smaller than the shear strength between the FRP matrix and FRP core bar, the failure will occur at the concrete-matrix interface (interface 1, as shown in Figure 9). In contrast, when the shear strength between the FRP matrix and FRP core bar is smaller than the shear strength between concrete and FRP matrix, failures occur at the FRP core bar-matrix interface (interface 2, as shown in Figure 9). In the case of normal concrete strength, the failure will mostly occur at interface 1, while with high concrete strength, the failure would shift to interface 2. Both interfaces are identified in Figure 9.

4.1.6 Bond strength prediction

As mentioned earlier, analytical predictions for determining the bond strength between FRP bar and concrete are still scarce. These formulas are essential to improve the knowledge on the bond characteristics between FRP bars and concrete and are necessary for the design of reinforced concrete structures with FRP bars. To predict the bond strength between steel bars and concrete, there are several equations, such as those presented in [38]. However, for the bond between FRP bars and concrete, a few bond strength prediction equations are available. The ACI 440.1R-15 [4] guidelines include an equation for predicting the bond strength; however the equation is based on beam bond tests. Two formulas available in the literature were selected for the simulation of the data collected in the present work (based on pullout tests). The first, from *fib* Bulletin 55 [35] [Eqs. (3) and (4)], is commonly used for deformed steel bars and considers that the bond strength increases proportionally to the compressive strength of concrete f_{ck}. Failure mode (pullout or splitting) is also considered. A second formula proposed by Okelo and Yuan [34] [Eq. (5)] was also selected. This equation accounts for the influence of the concrete strength and the FRP bar diameter $Ø_b$:

$$\tau_{\max} = 2.5\sqrt{f_{\mathrm{ck}}} \qquad \text{for pullout failure} \tag{3}$$

$$\tau_{\max} = 7.0\left(\frac{f_{\mathrm{ck}}}{20}\right)^{0.25} \qquad \text{for splitting failure} \tag{4}$$

$$\tau_{\max} = 14.7\frac{\sqrt{f_{\mathrm{ck}}}}{\emptyset_{\mathrm{b}}} \tag{5}$$

Figure 10 shows the predicted bond strength *versus* the experimental data for both formulations. In this analysis only specimens with an embedded length of 5Ø were considered. For the ideal prediction, the data points must coincide with the 45-degree dashed line (i.e., equality line). However, for the present case it becomes clear that in general a significant dispersion is observed, especially when the Okelo and Yuan proposal is used. Error metrics were used to assess the accuracy of both proposals, namely mean absolute error (MAE) and root mean squared error (RMSE). Those are defined in Eqs. (6) and (7), respectively. In these equations, $\tau_{\mathrm{max,calc}}$ is the calculated bond strength, $\tau_{\mathrm{max,exp}}$ is the experimental bond strength, and n is the number of specimens. Table 2 presents the obtained results. The dispersion observed in Figure 10 was confirmed by the high error values found, primarily when the Okelo and Yuan proposal was used.

$$\mathrm{MAE} = \frac{1}{n}\sum_{i=1}^{n}\left|\left(\tau_{\mathrm{max,calc}}\right)_i - \left(\tau_{\mathrm{max,exp}}\right)_i\right| \tag{6}$$

$$\mathrm{RMSE} = \sqrt{\frac{1}{n}\sum_{i=1}^{n}\left[\left(\tau_{\mathrm{max,calc}}\right)_i - \left(\tau_{\mathrm{max,exp}}\right)_i\right]^2} \tag{7}$$

Given the low accuracy of the existing formulas, a new proposal is given in the scope of the present work. From the analysis carried out in the previous sections, it was concluded that (i) the concrete strength and (ii) the type of FRP bar surface treatment are the critical parameters influencing the bond strength. Based on that, Eq. (8) is proposed to predict the bond strength, as a function of FRP bar treatment:

$$\tau_{max} = \alpha(f_{ck})^{\beta} \quad (8)$$

Thus, the parameters α and β were determined for specimens with an embedded length of 5Ø and a given FRP bar surface treatment type, using the Nonlinear Least Squares method.

Table 3 presents the values obtained for α and β, while Table 2 includes the corresponding error metrics. Figure 11 shows the comparison between the bond strength predicted values *versus* experimental results. From these results, in general, much better predictions were obtained with reduced errors.

4.2 Specimens under aging conditions

Existing literature includes a reduced number of studies on durability issues of the bond between FRP bars and concrete. The bond durability has been evaluated through accelerated aging tests, using different exposure environments under specific temperature and time of exposure. The information collected allowed the analysis of different environments, namely: (i) acid solution (AC), (ii) alkaline solution (AK), (iii) saline solution (SA), (iv) immersion in water (WA), (v) elevated temperature in a dry environment (HT), elevated temperature in a dry environment followed by immersion (vi) in water (HWA), or (vii) in saline solution (HSA), and (viii) thermal cycles (TC).

4.2.1 Exposure temperature effect

High temperatures can be used to accelerate the aging of specimens that are subjected to adverse exposure environments. However, the properties of the materials must be known, and their limits respected. For materials that use polymeric matrices, such as FRP bars, the temperature used for accelerating the aging must be far from the glass transition temperature (T_g). The ACI 440.1R-15 [4] guidelines present indicative T_g values between 93 °C and 120 °C for FRP bars. On the other hand, some authors, e.g., [14, 23, 25, 29, 30], reported values of FRP bars T_g between 103 °C and 129 °C. In these cases, different types of resins (epoxy and vinyl ester), and FRP (GFRP, BFRP, and CFRP) were considered. However, in many other works [19 – 22, 24, 26 – 28] no values of T_g were reported. It is known that high temperatures can affect the physical properties of the material, e.g., the thermal expansion coefficient [39]. The JRC report [40] indicates that the service temperature must be at least 20 °C lower than the glass transition temperature. Therefore, a temperature of 80 °C was adopted as the upper limit of temperature used in the tests, ensuring that it is at least 20 °C lower than the glass transition temperature reported

in the database for the FRP bars. Thus, all the tests that used temperatures outside these limits were disregarded in this study.

The retention of the bond strength as a function of the temperature is shown in Figure 12. For each environmental condition, the retention was evaluated against the control specimen. In general, there is no correlation between the bond strength retention and the increase of the temperature. Data show a substantial dispersion amongst experiment results, with several unexpected retention values, higher than 100%. This may be explained by the improvement of concrete properties (curing) consequent to the synergic effects of water immersion and temperature.

Figure 12a shows the bond strength retention for different exposure temperatures for the specimens subjected to immersion conditions. Three exposure temperatures were evaluated for the acid solution: room temperature, 60 °C, and 80 °C. In acid solution, the bond strength retention varied between 69% and 91%, with the minimum retention obtained for exposure to 80 °C (69%), and the maximum at 60 °C (91%). Exposure to alkaline solution generated bond strength retention between 81% (at 80 °C) and 123% (at 60 °C). The studied temperatures for immersion in alkaline solution were room temperature, 40 °C, 50 °C, 60 °C, and 80 °C. The accelerated aging of specimens exposed to the saline solution was performed at room temperature, 40 °C, 50 °C, 60 °C, and 70 °C. In this environment, bond strength retentions between 74% at (60 °C) and 129% (at room temperature) were obtained. Immersion in water caused bond strength retention from 76% (at room temperature) to 106% (at 60 °C). Room temperature, 40 °C, 50 °C, 60 °C, and 80 °C were used for immersion in water.

For the other environmental exposure conditions (Figure 12b), the temperature played a fundamental role in the specimens aging. The bond strength retention of specimens subjected to elevated temperature in a dry environment (40 °C, 60 °C, and 80 °C) varied between 89% and 103%, both for the highest temperature. Similar results were observed with the thermal cycles; the bond strength retentions varied between 81% and 100%. The exposure of specimens to elevated temperature (80 °C) in a dry environment, followed by immersions, generated bond strength retentions between 80% and 94% for immersion in water, and between 70% and 89% for immersion in saline solution.

When considering all the analyzed exposures, it is concluded that the exposure to the saline solution caused lower levels of degradation than other exposures, with an average bond strength retention of 99%. On the other hand, the

worst result was found for elevated temperature followed by saline immersion. In this condition (HSA), the bond strength retention was 80%.

The analysis considering the increase in temperature includes results from different exposure times (from 7 to 240 days), causing a large dispersion of the data, as seen in Figure 12. However, regardless of this dispersion, the results consistently show high retention values, i.e., above 70%. A more all-encompassing analysis is made in Section 5, where temperature and exposure time are considered simultaneously.

4.2.2 Exposure time effect

In the context of durability, time is an essential factor to be considered. From the data collected, the exposure times for which the bond specimens were subjected to the accelerated aging environments vary from 7 to 240 days (5760 hours of exposure). Similarly, as done for temperature, the bond strength retention was calculated, considering the increase in the exposure time. The retention of the bond strength concerning the exposure time is shown in Figure 13; again, remarkable dispersion of the results is noted.

The influence of time on the bond strength for immersion solutions is seen in Figure 13a. Exposures between 720 and 2160 hours resulted in bond strength retention ranging from 69% (720 h) to 114% (1440 h) when the acid solution was used. The bond strength retention in an alkaline environment varied between 75% (2160 h) and 115% (1080 h). The alkaline solution was used in periods from 720 to 4320 hours. Saline aging was carried out in between 360 and 2160 hours; in this period, the bond strength showed retentions ranging from 74% (2160 h) to 122% (720 h). Finally, immersion in water resulted in bond strength retention between 76% (2160 h) and 104% (2160 h) for periods of exposure between 720 and 4320 hours.

In Figure 13b the other exposure cases are considered to verify the exposure time influence on bond strength. Periods of 2160, 2880, and 5760 hours were used for aging at elevated temperature (HT). In this case, bond strength retentions between 93% and 103% were observed, both for the 2160 hours exposure period. The use of elevated temperature followed by immersions was done for 2160 hours, with the first 1440 hours under exposure to elevated temperature, followed by 720 hours of immersion (water or saline solution). Retentions between 80% and 94% were verified for HWA, while in HSA the retention varied between 70% and 89%. The durability was also evaluated throughout thermal cycles. The duration of each thermal cycle varied between 5 h and 24 h, being in total between 168 and 2568 hours. The bond strength retentions were between 81% (2568 h) and 103% (168 h) under the influence of thermal cycles.

Again, the assessment of all exposure environments showed that immersion in saline solution exhibited better results, with an average bond strength retention of 97%. On the other hand, exposure to high temperature followed by saline immersion showed the lowest bond strength retention (80%).

For each environment considered to analyze the effect of increased exposure time, temperatures between 20 °C and 80 °C were included. This temperature range can cause more data dispersion. Despite this, the results are consistent, with retentions above 70%. A more detailed analysis considering the effect of both temperature and time of exposure is made in Section 5.

In addition to the bond strength analysis, the degradation mechanisms of the conditioned specimens were observed and compared with the unconditioned specimens after the direct pullout tests. In general, no changes in the failure mode of the specimens were reported. However, Yan et al. [25] indicated changes in the failure mode from pullout failure to concrete splitting after exposure to freeze-thaw cycles for specimens with a concrete cover of 3Ø. For larger concrete covers, changes in the failure mode were not highlighted, which indicates, according to the authors, that a concrete cover of 3Ø is not capable of resisting attacks caused by environmental agents.

Through visual analysis, some authors observed, after exposure, changes in the FRP bar surface color, e.g. [19, 28], or residual blisters from the FRP bar matrix on the concrete surface, e.g. [19, 20, 27]. Visual analyzes indicate that interlaminar shear between the FRP bar surface layers was observed after direct pullout tests for both conditioned and unconditioned specimens, e.g. [20, 25, 28]. El Refai et al. [20] reported a reduction in diameter for both conditioned and unconditioned specimens, reaching up to 50% reduction. Contradictory effects in microstructure analyzes have been also reported. Dong et al. [28] reported a clearly affected area with loose fibers embedded in the bar surface matrix after exposure to the saline environment. On the other hand, Robert and Benmokrane [23] indicated that exposure to the alkaline solution did not affect the microstructure properties of the GFRP.

5. LONG-TERM PREDICTION

Accounting for the long-term exposure to adverse environments and thus reducing the bond strength between FRP bars and concrete for the desired service life is necessary in order to guarantee the structural safety of the reinforcement. In this section, the bond strength of the FRP bars to concrete is predicted according to the method described in the *fib* bulletin 40 [1].

The step-by-step procedure to determine the long-term prediction of bond strength retention was plotted in the flowchart shown in Figure 14. The first step is to determine a degradation curve for each exposure environment and, at each temperature, fitting a straight line (power equation) on a double logarithmic scale, as shown in Figure 15. As a second step, all lines with an upward trend are discarded from the analysis, as the upward values can be unrealistic and do not guarantee that the bond strength predicted is safe. The third step is to determine the slope (m) of each valid degradation curve. Then, in the fourth step, the average of the slopes $(\bar{m})$ is determined. The fifth step is the determination of the standard reduction in percent per decade due to environmental influence (R_{10}), shown in Figure 15; for this, it is assumed that the rate of degradation is similar regardless of the environment, as done in [41]. Then, in the sixth step, the influence term (n) is determined according to the desired moisture, temperature, and service life parameters (Table 4). It is suggested that the bond strength be reduced by an environmental reduction factor for bond strength $\left(\eta_{\mathrm{env,b}}\right)$, which is defined in the seventh step, shown in the flowchart, according to Eq. (9). Finally, the bond strength retention $\left({}^{1}/_{\eta_{\mathrm{env,b}}}\right)$ can be determined:

$$\eta_{\mathrm{env,b}} = \frac{1}{\left(\frac{100 - R_{10}}{100}\right)^{n}} \tag{9}$$

Following the steps presented in the flowchart (Figure 14) and described above, each exposure environment, at each temperature, was fitted with a straight line on a double logarithmic scale (Figure 16). Two of the eight environments available for analysis were not considered. Both environments comprised results for only 90 days of exposure, thus making perform the abovementioned procedure inviable. Due to retentions above 100%, i.e., bond strengths higher on aged specimens than on the control specimens, some fitting showed an upward trend, such as the fit for the acid environment at 60 °C (Figure 16a). Thus, according to what was presented in the flowchart (second step), these results were excluded from the analysis, to ensure safety.

Then, the slopes (m) of the remaining curves and its average ($\bar{m}$) were calculated. The values obtained are shown in Table 5. After, assuming that the rate of degradation was similar for any environment, using the average value of the slopes ($\bar{m}$), R_{10} was calculated ($R_{10} = 12.8\%$). According to the flowchart (Figure 14), the next step consisted on the determination of n. In this study, the service life was fixed at 50 years, and all parameters of moisture (RH) and mean annual temperature (MAT) were used.

With the values of R_{10} and n determined, the environmental reduction factors for bond strength $\left(\eta_{\mathrm{env,b}}\right)$ and its respective bond strength retentions $\left({}^{1}/_{\eta_{\mathrm{env,b}}}\right)$ were calculated. The retention results obtained for a service life of 50 years and varying moisture and temperature conditions are shown in Table 6. The bond strength retention after 50 years of service life ranges from 53% to 85%. Figure 17 shows the bond strength retention results after 50 years of service life, considering the MAT between 25 °C and 35 °C. For dry, moist, and saturated conditions, 69%, 60%, and 53% retentions were observed, respectively.

A comparison between the tensile strength retention of FRP bars and the bond strength retention of FRP bars to concrete was performed using the results obtained here and comparing them with the retentions obtained by Serbescu et al. [41]. Serbescu et al. used the *fib* Bulletin 40 [1] method to determine the tensile strength retention prediction of BFRP bars after 100 years of service life. For a direct comparison, the bond strength retention prediction was also performed for 100 years. The result obtained was a bond strength retention of 54%, considering the saturated moisture condition and MAT between 15 °C and 25 °C. The tensile strength retention obtained by Serbescu et al. [41] in the saturated condition at 20 °C was 62%; these results are shown in Figure 18. As expected, the bar tensile strength retention is superior but not so far from the bond strength retention. Further studies are needed to determine whether there is a correlation between the tensile strength retention and bond strength retention for FRP bar and how these two degradations should be combined to obtain safe and reliable predictions of the FRP reinforcing bar performance.

6. CONCLUSIONS

This paper had the main objective of investigating several parameters that can interfere in the bond strength between FRP bars and concrete. Additionally, the experimental results collated in the database were used to make long-term predictions of bond durability, according to the *fib* Bulletin 40 method. From the analyzes carried out, the following conclusions can be drawn:

i. Several components of the database have wide variations, such as bond strength from 0.1 MPa to 67.8 MPa, FRP bar Young's modulus from 31 GPa to 170 GPa, and compressive strength of concrete from 12 MPa to 170 MPa;

ii. The type of fiber and the FRP bar diameter have no relevant influence on the normalized bond strength. When axial stiffness is considered, CFRP had the lowest bond strength, while BFRP the greatest benefit, as they lead to higher bond strength with respect to GFRP and CFRP;

iii. Because of the nonlinear distribution of the shear stresses along the embedded length and the Poisson's ratio effect, the higher the embedded length analyzed, the lower the bond strength. This observation was previously also reported in the literature;

iv. Surface treatments (e.g., deformed and/or sand coated surfaces) improve the bond strength. While bars with smooth surfaces have very low bond strength values and are therefore not recommended for use as reinforcement in concrete structures;

v. The suggested equation to determine the bond strength, considering the different type of FRP bar surfaces, presents better predictions for the bond strength of the FRP bars to concrete than those found in the bibliographic review carried out;

vi. For exposure environments (acid solution, alkaline solution, saline solution, immersion in water, high temperature, high temperature followed by immersions and thermal cycles), exposure times (up to a maximum of 5760 hours), and exposure temperatures (20 °C to 80 °C), low levels of bond degradation were found, with very high retention rates, that is, close to 100%;

vii. A long-term prediction of bond durability was performed according to the *fib* bulletin 40 method, adopting a similar degradation rate, regardless of the environment. For 50 years of service, retentions from 53% to 85% of the bond strength were found in dry, moist, and saturated conditions.

479 From the data collated and analyzed in this study, the use of FRP bars as reinforcement in concrete structures does

480 not seem to present critical issues, even when exposed to harsh environments with a high degree of degradation.

ACKNOWLEDGEMENTS

The study presented in this paper is a part of the research project "EcOffShorBE – Eco Offshore Built Environment", financed by FEDER funds in the scope of the EcOffShorBE project (NORTE-01-0247-FEDER-037417). The first and second authors wish also to acknowledge the grants no. DFA/BD/6484/2020 and SFRH/BSAB/150266/2019, respectively, provided by FCT.

REFERENCES

[1] FIB - Fédération Internationale du Béton, "fib Bulletin 40, FRP reinforcement in RC structures," Lausanne, Switzerland, 2007.

[2] J. Sena-Cruz, J. Barros, M. Coelho and C. Pellegrino, "Advancements in retrofitting reinforced concrete structures by the use of CFRP materials," in *Structural rehabilitation of old buildings*, Springer, 2014, pp. 259-284.

[3] J. Sena-Cruz, J. A. Barros and S. J. Dias, "First seminar on the design of strengthening of RC structures with FRP materials" University of Minho, Department of Civil Engineering, 2011, 66 pp. (in Portuguese)

[4] ACI 440.1R-15, "Guide for the Design and Construction of Structural Concrete Reinforced with Fiber-Reinforced Polymer (FRP) Bars," American Concrete Institute, Farmington Hills, United States of America, 2015.

[5] CSA S806-12, "Design and construction of building structures with fibre-reinforced polymers," Canadian Standards Association, Mississauga, Canada, 2012.

[6] CNR 203-06, "Guide for the Design and Construction of Concrete Structures Reinforced with Fiber-Reinforced Polymer Bars," Rome, Italy, 2007.

[7] ASTM D7913/D7913M-14, "Standard test method for bond strength of fiber-reinforced polymer matrix composite bars to concrete by pullout testing," ASTM International, West Conshohocken, United States of America, 2020.

[8] ACI 440.3R-04, "Guide test methods for fiber-reinforced polymers (FRPs) for reinforcing or strengthening concrete structures," American Concrete Institute, Farmington Hills, United States of America, 2004.

[9] M. A. Aiello, M. Leone and M. Pecce, "Bond performances of FRP rebars-reinforced concrete," *Journal of materials in civil engineering,* vol. 19, no. 3, pp. 205-213, 2007.

[10] M. Baena, L. Torres, A. Turon and C. Barris, "Experimental study of bond behaviour between concrete and FRP bars using a pull-out test," *Composites Part B: Engineering,* vol. 40, no. 8, pp. 784-797, 2009.

[11] Z. Achillides and K. Pilakoutas, "Bond behavior of fiber reinforced polymer bars under direct pullout conditions," *Journal of Composites for construction,* vol. 8, no. 2, pp. 173-181, 2004.

[12] S. A. Firas, F. Gilles and L. R. Robert, "Bond between carbon fibre-reinforced polymer (CFRP) bars and ultra high performance fibre reinforced concrete (UHPFRC): Experimental study," *Construction and Building Materials,* vol. 25, no. 2, pp. 479-485, 2011.

[13] A. El Refai, M.-A. Ammar and R. Masmoudi, "Bond performance of basalt fiber-reinforced polymer bars to concrete," *Journal of Composites for Construction,* vol. 19, no. 3, p. 04014050, 2015.

[14] S. U. Al-Dulaijan, M. M. Al-Zahrani, A. Nanni, C. E. Bakis and T. E. Boothby, "Effect of environmental pre-conditioning on bond of FRP reinforcement to concrete," *Journal of Reinforced Plastics and Composites,* vol. 20, no. 10, pp. 881-900, 2001.

[15] M. Harajli and M. Abouniaj, "Bond performance of GFRP bars in tension: Experimental evaluation and assessment of ACI 440 guidelines," *Journal of Composites for Construction,* vol. 14, no. 6, pp. 659-668, 2010.

[16] V. A. Rossetti, D. Galeota and M. Giammatteo, "Local bond stress-slip relationships of glass fibre reinforced plastic bars embedded in concrete," *Materials and Structures,* vol. 28, no. 6, pp. 340-344, 1995.

[17] J.-Y. Lee, T.-Y. Kim, T.-J. Kim, C.-K. Yi, J.-S. Park, Y.-C. You and Y.-H. Park, "Interfacial bond strength of glass fiber reinforced polymer bars in high-strength concrete," *Composites Part B: Engineering,* vol. 39, no. 2, pp. 258-270, 2008.

[18] B. Kim, J.-H. Doh, C.-K. Yi and J.-Y. Lee, "Effects of structural fibers on bonding mechanism changes in interface between GFRP bar and concrete," *Composites Part B: Engineering,* vol. 45, no. 1, pp. 768-779, 2013.

[19] A. Altalmas, A. El Refai and F. Abed, "Bond degradation of basalt fiber-reinforced polymer (BFRP) bars exposed to accelerated aging conditions," *Construction and Building Materials,* vol. 81, pp. 162-171, 2015.

[20] A. El Refai, F. Abed and A. Altalmas, "Bond durability of basalt fiber-reinforced polymer bars embedded in concrete under direct pullout conditions," *Journal of Composites for Construction,* vol. 19, no. 5, p. 04014078, 2014.

[21] A. Belarbi and H. Wang, "Bond durability of FRP bars embedded in fiber-reinforced concrete," *Journal of Composites for Construction,* vol. 16, no. 4, pp. 371-380, 2012.

[22] J. F. Davalos, Y. Chen and I. Ray, "Effect of FRP bar degradation on interface bond with high strength concrete," *Cement and Concrete Composites,* vol. 30, no. 8, pp. 722-730, 2008.

[23] M. Robert and B. Benmokrane, "Effect of aging on bond of GFRP bars embedded in concrete," *Cement and concrete composites,* vol. 32, no. 6, pp. 461-467, 2010.

[24] R. Masmoudi, A. Masmoudi, M. B. Ouezdou and A. Daoud, "Long-term bond performance of GFRP bars in concrete under temperature ranging from 20 °C to 80 °C," *Construction and Building Materials,* vol. 25, no. 2, pp. 486-493, 2011.

[25] F. Yan, Z. Lin, D. Zhang, Z. Gao and M. Li, "Experimental study on bond durability of glass fiber reinforced polymer bars in concrete exposed to harsh environmental agents: freeze-thaw cycles and alkaline-saline solution," *Composites Part B: Engineering,* vol. 116, pp. 406-421, 2017.

[26] J. Zhou, X. Chen and S. Chen, "Durability and service life prediction of GFRP bars embedded in concrete under acid environment," *Nuclear Engineering and Design,* vol. 241, no. 10, pp. 4095-4102, 2011.

[27] J. Zhou, X. Chen and S. Chen, "Effect of different environments on bond strength of glass fiber-reinforced polymer and steel reinforcing bars," *KSCE Journal of Civil Engineering,* vol. 16, no. 6, pp. 994-1002, 2012.

[28] Z. Dong, G. Wu, B. Xu, X. Wang and L. Taerwe, "Bond durability of BFRP bars embedded in concrete under seawater conditions and the long-term bond strength prediction," vol. 92, pp. 552-562, 2016.

[29] F. Yan and Z. Lin, "Bond durability assessment and long-term degradation prediction for GFRP bars to fiber-reinforced concrete under saline solutions," *Composite Structures,* vol. 161, pp. 393-406, 2017.

[30] M. Hassan, B. Benmokrane, A. ElSafty and A. Fam, "Bond durability of basalt-fiber-reinforced-polymer (BFRP) bars embedded in concrete in aggressive environment," *Composites Part B: Engineering,* vol. 106, pp. 262-272, 2016.

[31] Q. W. Bi, Q. X. Wang and H. Wang, "Study on Bond Properties of BFRP Bars to Basalt Fiber Reinforced Concrete," *Advanced Materials Research,* vol. 163, pp. 1251-1256, 2011.

[32] M. R. Ehsani, H. Saadatmanesh and S. Tao, "Bond behavior of deformed GFRP rebars," *Journal of Composite Materials,* vol. 31, no. 14, pp. 1413-1430, 1997.

[33] O. Chaallal and B. Benmokrane, "Pullout and bond of glass-fibre rods embedded in concrete and cement grout," *Materials and structures,* vol. 26, no. 3, pp. 167-175, 1993.

[34] R. Okelo and R. L. Yuan, "Bond strength of fiber reinforced polymer rebars in normal strength concrete," *Journal of composites for construction,* vol. 9, no. 3, pp. 203-213, 2005.

[35] FIB - Fédération Internationale du Béton, "fib Bulletin 55, Model Code 2010," Lausanne, Switzerland, 2010.

[36] T. D'Antino, M. Pisani and C. Poggi, "Effect of the environment on the performance of GFRP reinforcing bars," *Composites Part B: Engineering,* vol. 141, pp. 123-136, 2018.

[37] E. Cosenza, G. Manfredi and R. Realfonzo, "Behavior and modeling of bond of FRP rebars to concrete," *Journal of composites for construction,* vol. 1, pp. 40-51, 1997.

[38] Y. Kim, J. Sim and C. Park, "Mechanical properties of recycled aggregate concrete with deformed steel re-bar," *Journal of marine science and technology,* vol. 20, no. 3, pp. 274-280, 2012.

[39] M. Robert, P. Wang, P. Cousin and B. Benmokrane, "Temperature as an accelerating factor for long-term durability testing of FRPs: Should there be any limitations?," *Journal of Composites for Construction,* pp. 361-367, 2010.

[40] L. Ascione, J.-F. Caron, P. Godonou, K. van IJselmuijden, J. Knippers, T. Mottram, M. Oppe, M. Gantriis Sorensen, J. Taby and L. Tromp, "Prospect for new guidance in the design of FRP: Support to the implementation, harmonization and further development of the Eurocodes," Publications Office of the European Union, 2016.

[41] A. Serbescu, M. Guadagnini and K. Pilakoutas, "Mechanical Characterization of Basalt FRP Rebars and Long-Term Strength Predictive Model," *Journal of Composites for Construction,* vol. 19, p. 04014037, 2015.

487

TABLE CAPTIONS

Table 1: Summary of the analyzed parameters in the database.

Table 2: Error metrics obtained in the prediction models.

Table 3: Parameters α and β obtained.

Table 4: Degradation terms (adapted from [1]).

Table 5: Slopes of the degradation curves.

Table 6: Bond strength retention prediction after 50 years of service life according to fib Bulletin 40 method.

497 **Table 1:** Summary of the analyzed parameters in the database.

Parameter	Range/type	No. of pullout results
Type of FRP	GFRP	598
	BFRP	251
	CFRP	153
Diameter [mm]	≥ 7 to < 8	4
	≥ 8 to < 9	229
	≥ 9 to < 10	52
	≥ 10 to < 12	57
	≥ 12 to < 13	461
	≥ 13 to < 14	64
	≥ 14 to < 16	12
	≥ 16 to < 18	61
	≥ 18 to < 19	12
	≥ 19 to < 21	30
	≥ 21 to < 25	2
	≥ 25 to < 29	12
	≥ 29 to < 30	6
Embedded length [nØ]	≥ 2 to < 5	112
	5	681
	> 5 to < 8	72
	≥ 8 to < 10	58
	≥ 10 to < 15	51
	15	17
	> 15 to < 20	6
	20	5
Surface treatment	Sand-coated + deformed surface	337
	Deformed surface	494
	Sand-coated	130
	Smooth	41
Environment	Unconditioned	564
	Acid solution	33
	Alkaline solution	72
	Saline solution	205
	Water immersion	48
	Elevated temperature	21
	Temperature + water	9
	Temperature + saline	9
	Thermal cycles	41

Concrete compressive strength range [MPa]	12 to 170 (46.5)	1002
Bond strength [MPa]	0.1 to 67.8 (16.2)	1002

Note: values in brackets are the averages

Table 2: Error metrics obtained in the prediction models.

Surface treatment	*fib* 55		Okelo and Yuan		Proposal	
	MAE	RMSE	MAE	RMSE	MAE	RMSE
SC + DS	4.77	6.42	10.52	11.49	3.26	4.60
DS	6.87	9.29	11.08	13.54	5.79	8.89
SC	4.04	4.69	8.14	9.09	4.23	5.19
SM	7.51	7.76	3.19	4.36	2.72	3.11

Table 3: Parameters α and β obtained.

Type of surface	α	β
SC + DS	5.24	0.33
DS	2.57	0.54
SC	3.33	0.41
SM	0.18	0.96

Table 4: Degradation terms (adapted from [1]).

Degradation term	Criterion	Value
n_{mo} – Moisture (RH)	Dry (50%)	− 1
	Moist (80%)	0
	Saturated (100%)	1
n_{T} – Mean annual temperature (MAT)	< 5 °C	− 0.5
	> 5 °C to < 15°C	0
	> 15 °C to < 25°C	0.5
	> 25 °C to < 35°C	1
n_{SL} – Desired service-life	1 year	1
	10 years	2

	50 years	2.7
	100 years	3

504

505 **Table 5:** Slopes of the degradation curves.

Environmental condition	Slope value (m)
AC 23 °C	−0.132
AK 40 °C	−0.050
AK 50 °C	−0.123
SA 23 °C	−0.047
SA 50 °C	−0.043
SA 60 °C	−0.024
SA 70 °C	−0.140
WA 40 °C	−0.057
WA 50 °C	−0.041
HT 40 °C	−0.003
HT 60 °C	−0.004
HT 80 °C	−0.088
TC −18 °C to 4 °C	−0.021
Average ($\overline{m}$)	−0.059

506

507 **Table 6:** Bond strength retention prediction after 50 years of service life according to *fib* Bulletin 40 method.

Moisture Condition (RH)	MAT	n	$\eta_{\text{env,b}}$	$1/\eta_{\text{env,b}}$
Dry (50%)	< 5 °C	1.2	1.18	85%
	> 5 °C to < 15°C	1.7	1.26	79%
	> 15 °C to < 25°C	2.2	1.35	74%
	> 25 °C to < 35°C	2.7	1.45	69%
Moist (80%)	< 5 °C	2.2	1.35	74%
	> 5 °C to < 15°C	2.7	1.45	69%
	> 15 °C to < 25°C	3.2	1.55	65%
	> 25 °C to < 35°C	3.7	1.66	60%
Saturated (100%)	< 5 °C	3.2	1.55	65%

	> 5 °C to < 15°C	3.7	1.66	60%
	> 15 °C to < 25°C	4.2	1.78	56%
	> 25 °C to < 35°C	4.7	1.90	53%

508

509

FIGURES CAPTIONS

Figure 1: Schematic of a typical test setup for bond characterization.

Figure 2: Influence of the fiber type on the normalized bond strength. Note: values near the bars are the mean values and the coefficients of variation (the latter in percentage).

Figure 3: Influence of the fiber type and bar stiffness on the normalized bond strength. Note: values near the bars are the mean values and the coefficients of variation (the latter in percentage).

Figure 4: Influence of the embedded length on the normalized bond strength. Note: values near the bars are the mean values and the coefficients of variation (the latter in percentage).

Figure 5: Exponential fitting of the relation between normalized bond strength and the embedded length.

Figure 6: Influence of the FRP bar diameter on the (a) normalized bond strength and (b) bond strength. Note: values near the bars are the mean values and the coefficients of variation (the latter in percentage).

Figure 7: Influence of the FRP bar surface on the normalized bond strength. Note: values near the bars are the mean values and the coefficients of variation (the latter in percentage).

Figure 8: Bond failure modes.

Figure 9: Interfacial bond failure (adapted from [15]).

Figure 10: Predicted vs. experimental bond strength: (a) fib bulletin 55 proposal; (b) Okelo and Yuan proposal.

Figure 11: Predicted vs. experimental bond strength using the proposed formula.

Figure 12: Influence of the temperature on the bond strength retention in (a) immersion solutions and (b) other environmental exposure conditions.

Figure 13: Influence of the time of exposure on the bond strength retention in (a) immersion solutions and (b) other environmetal exposure conditions.

Figure 14: Calculation flowchart for the fib bulletin 40 method.

Figure 15: Bond strength retention according to fib bulletin 40 (adapted from [1]).

Figure 16: Fitted curves for bond strength retention for (a) acid solution, (b) alkaline solution, (c) saline solution, (d) water immersion, (e) elevated temperature, and (f) thermal cycles.

Figure 17: Prediction of bond strength retention for 50 years of service life at 25 °C to 35 °C according to fib bulletin 40 method.

Figure 18: Comparison between FRP bar tensile strength retention and bond strength retention.

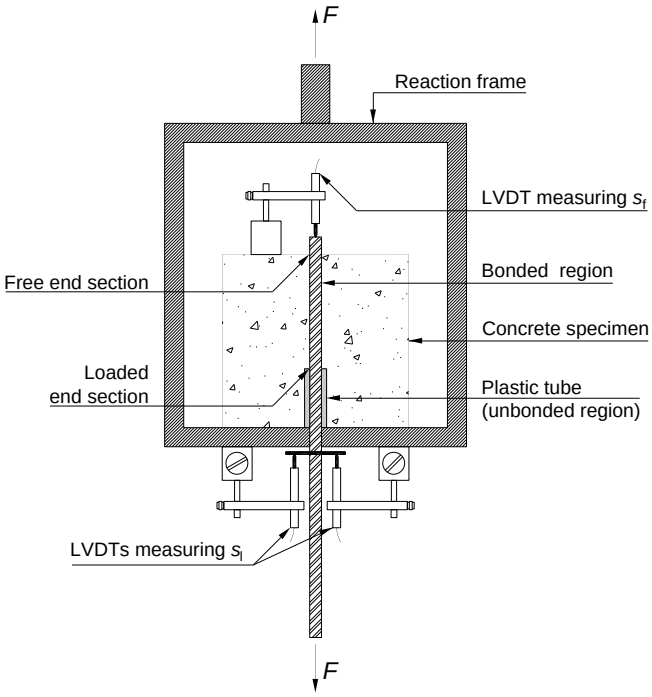


Figure 1: Schematic of a typical test setup for bond characterization.

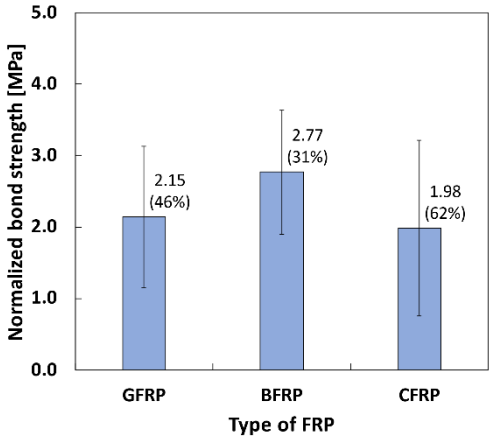


Figure 2: Influence of the fiber type on the normalized bond strength. Note: values near the bars are the mean values and the coefficients of variation (the latter in percentage).

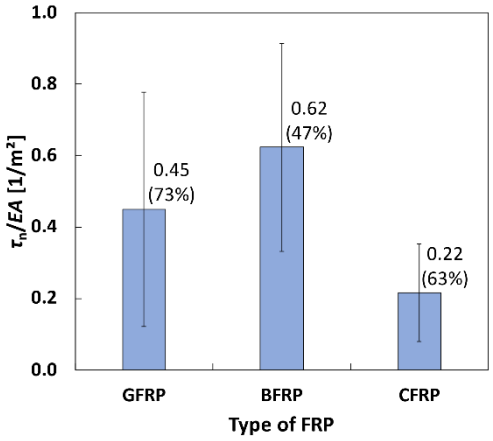


Figure 3: Influence of the fiber type and bar stiffness on the normalized bond strength. Note: values near the bars are the mean values and the coefficients of variation (the latter in percentage).

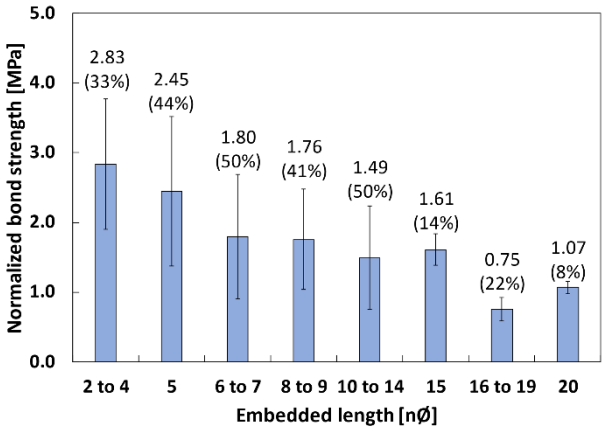
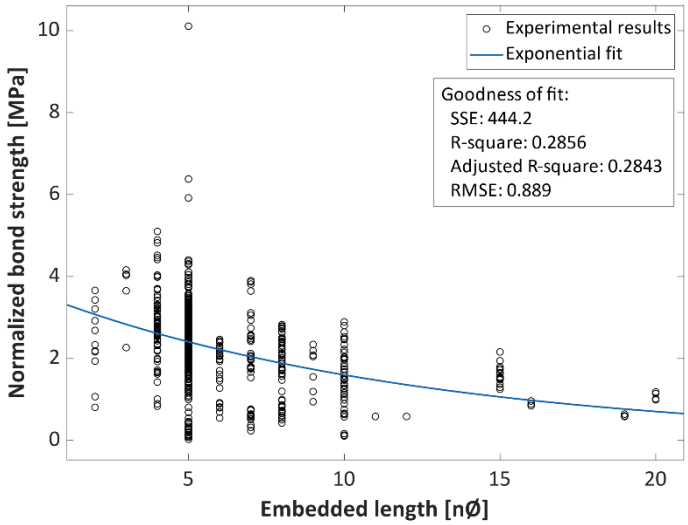


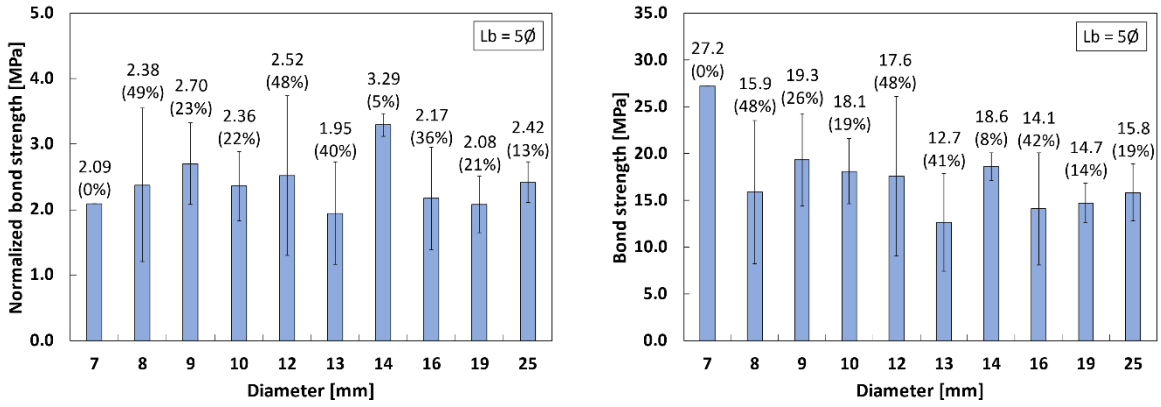
Figure 4: Influence of the embedded length on the normalized bond strength. Note: values near the bars are the mean values and the coefficients of variation (the latter in percentage).



554

555 **Figure 5:** Exponential fitting of the relation between normalized bond strength and the embedded length.

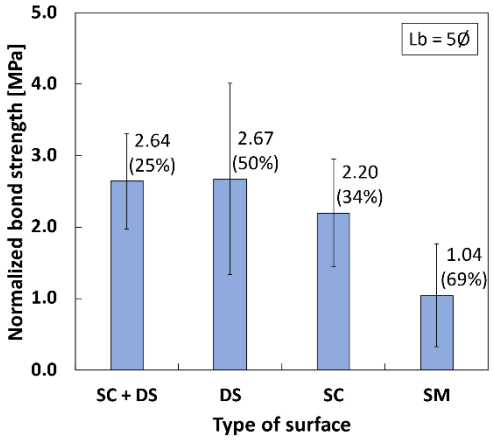
556



(a) (b)

557 **Figure 6:** Influence of the FRP bar diameter on the (a) normalized bond strength and (b) bond strength. Note:
558 values near the bars are the mean values and the coefficients of variation (the latter in percentage).

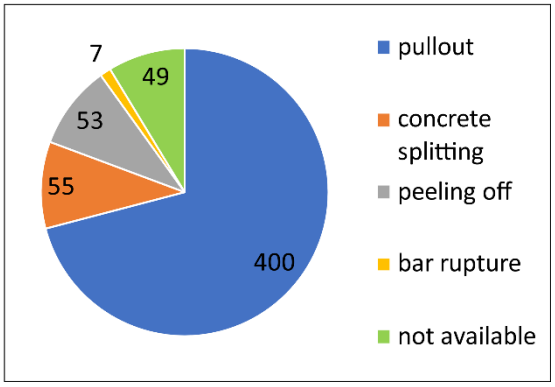
559



560

561 **Figure 7:** Influence of the FRP bar surface on the normalized bond strength. Note: values near the bars are the
562 mean values and the coefficients of variation (the latter in percentage).

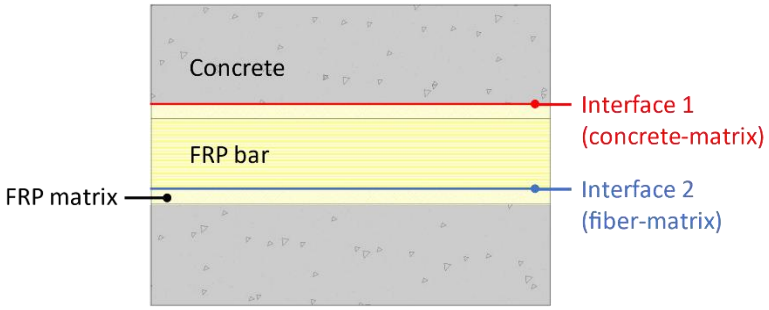
563



564

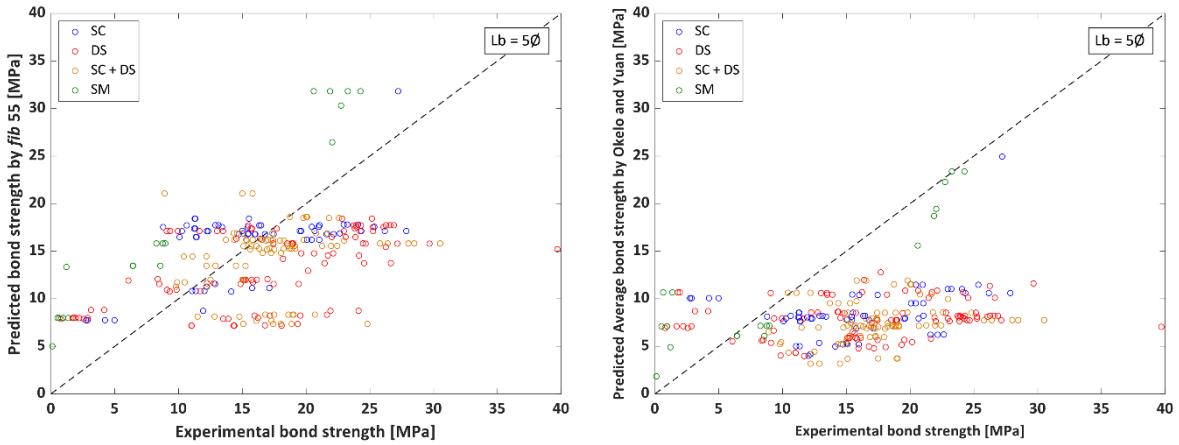
565 **Figure 8:** Bond failure modes.

566



567

568 **Figure 9:** Interfacial bond failure (adapted from [15]).



(a) (b)

Figure 10: Predicted *vs.* experimental bond strength: (a) *fib* bulletin 55 proposal; (b) Okelo and Yuan proposal.

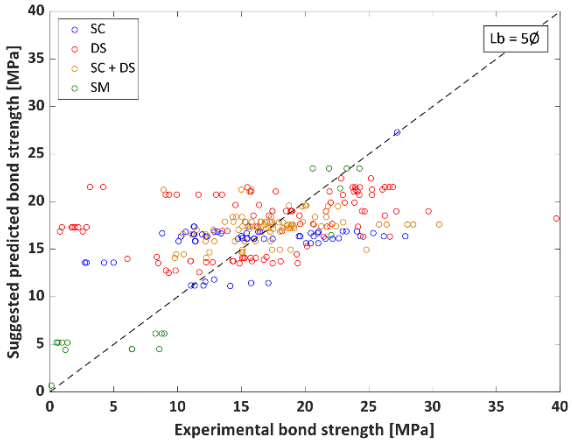
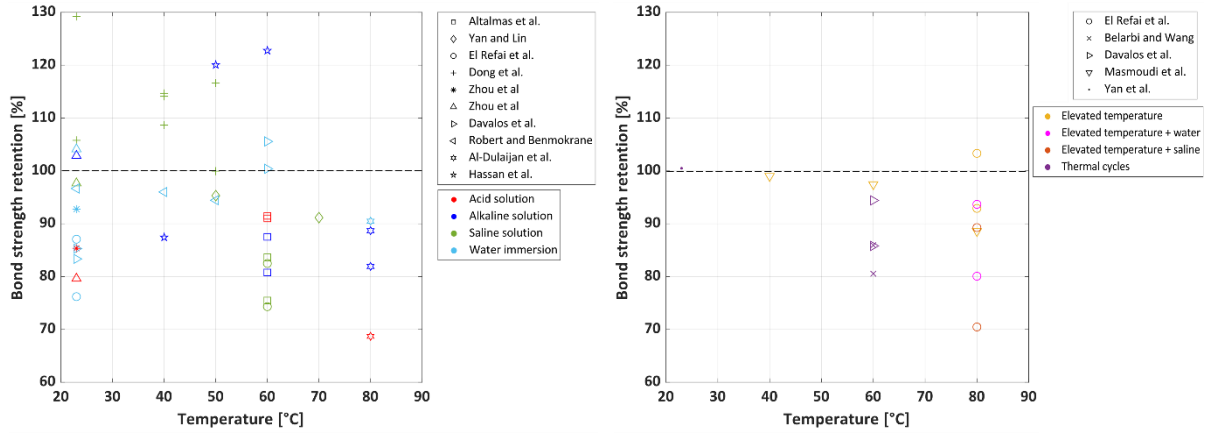
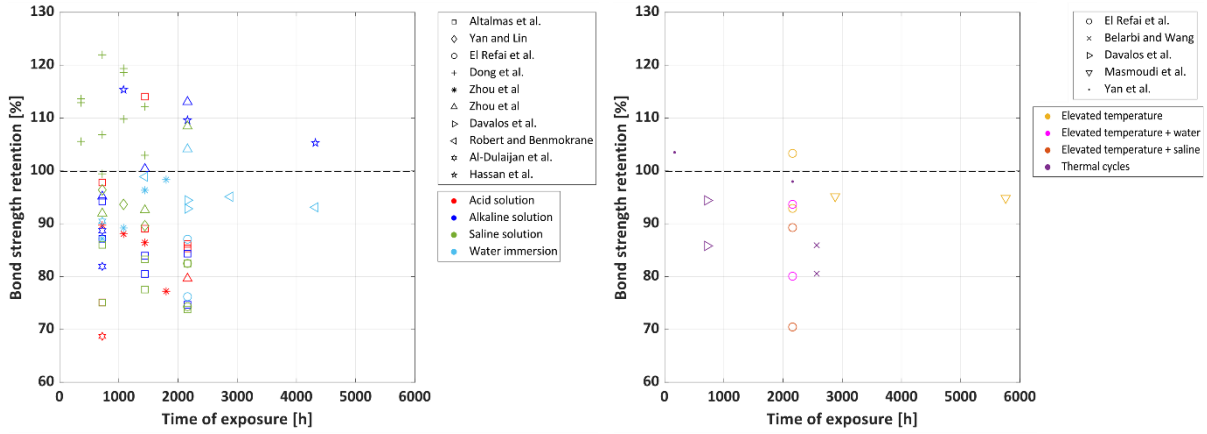


Figure 11: Predicted *vs.* experimental bond strength using the proposed formula.



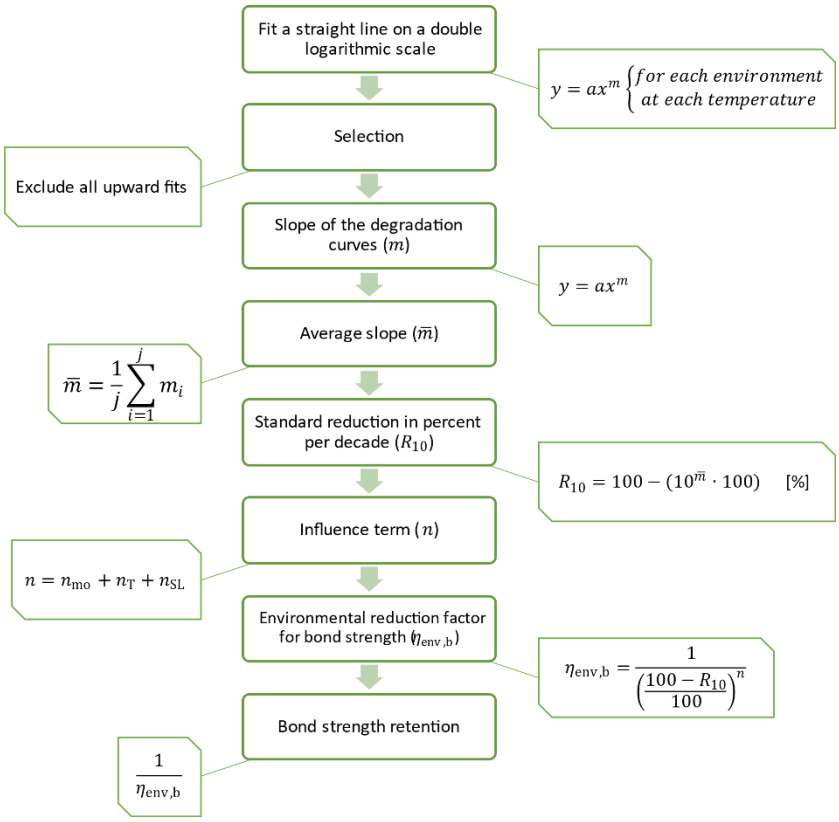
(a) (b)

Figure 12: Influence of the temperature on the bond strength retention in (a) immersion solutions and (b) other environmental exposure conditions.



(a) (b)

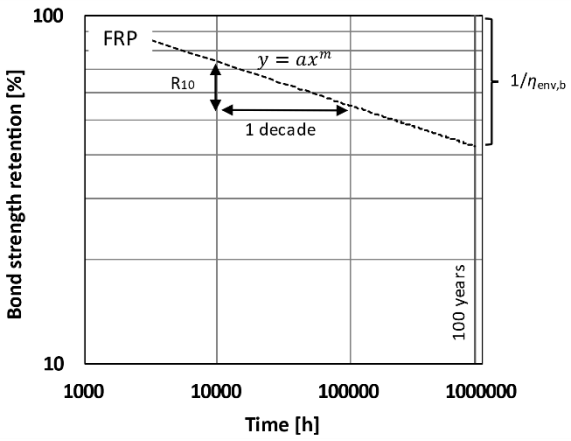
Figure 13: Influence of the time of exposure on the bond strength retention in (a) immersion solutions and (b) other environmetal exposure conditions.



581

582 **Figure 14:** Calculation flowchart for the *fib* bulletin 40 method.

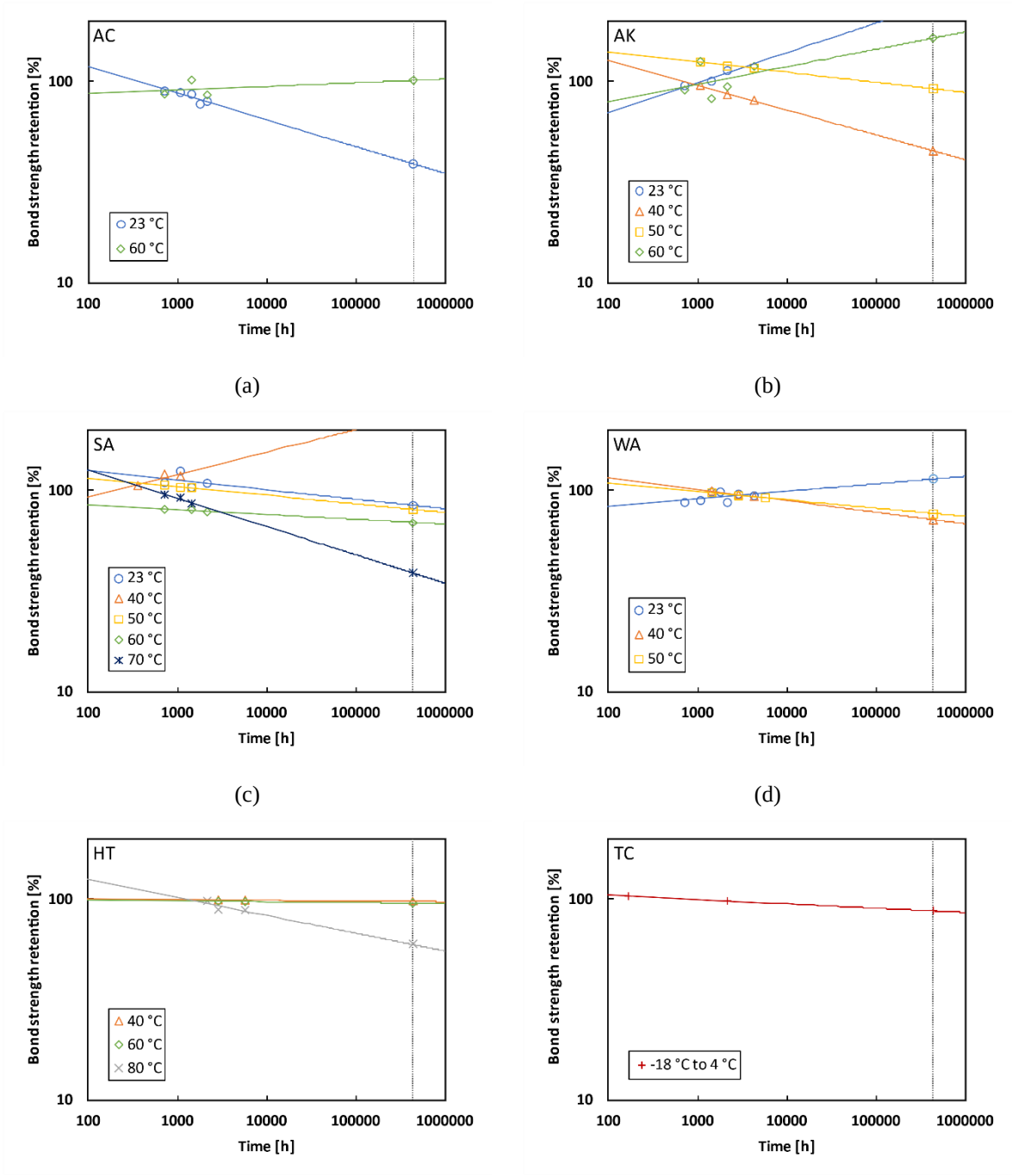
583



584

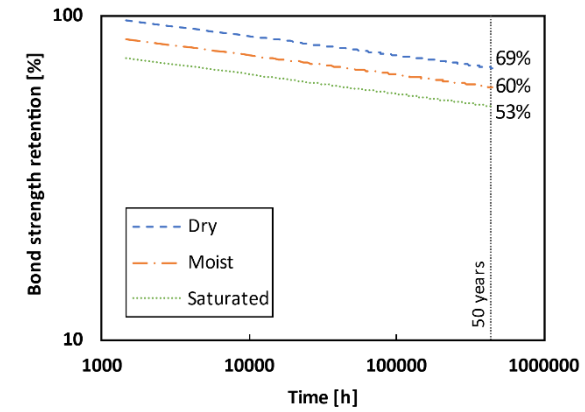
585 **Figure 15:** Bond strength retention according to *fib* bulletin 40 (adapted from [1]).

586



587 **Figure 16:** Fitted curves for bond strength retention for (a) acid solution, (b) alkaline solution, (c) saline
588 solution, (d) water immersion, (e) elevated temperature, and (f) thermal cycles.

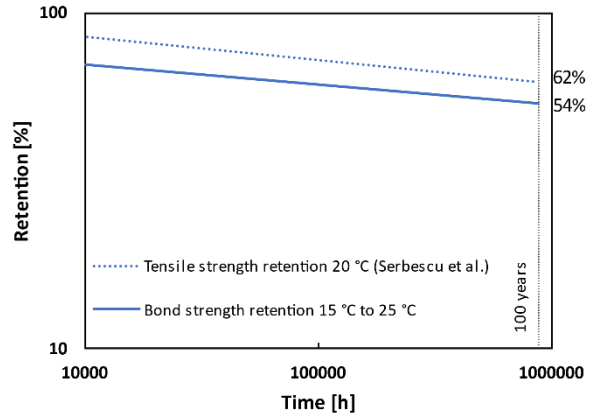
589



590

591 **Figure 17:** Prediction of bond strength retention for 50 years of service life at 25 °C to 35 °C according to *fib*
592 bulletin 40 method.

593



594

595 **Figure 18:** Comparison between FRP bar tensile strength retention and bond strength retention.